atmosphere

MDPI

Article

Monoterpene Chemical Speciation with High Time Resolution Using a FastGC/PTR-MS: Results from the COV^{3}ER Experiment on *Quercus ilex*

Sandy Bsaibes [1,2,*], Felix Piel [3,4,†], Valérie Gros [1,*], François Truong [1], Florence Lafouge [2], Raluca Ciuraru [2], Pauline Buysse [2], Julien Kammer [2,‡], Benjamin Loubet [2] and Michael Staudt [5]

1 Laboratoire des Sciences du Climat et de l'Environnement, LSCE, UMR CNRS-CEA-UVSQ, IPSL, Gif-sur-Yvette, 91191 Île-de-France, France; francois.truong@lsce.ipsl.fr
2 Institut National de Recherche Pour L'agriculture, L'alimentation et L'environnement, INRAe, UMR INRAe-AgroParisTech, Université Paris Saclay, Route de la Ferme, 78850 Thiverval-Grignon, France; florence.lafouge@inrae.fr (F.L.); raluca.ciuraru@inrae.fr (R.C.); pauline.buysse@inrae.fr (P.B.); julien.kammer@ucc.ie (J.K.); benjamin.loubet@inrae.fr (B.L.)
3 Ionicon Analytik GmbH, 6020 Innsbruck, Austria; felix.piel@kjemi.uio.no
4 Institute for Ion Physics and Applied Physics, University of Innsbruck, 6020 Innsbruck, Austria
5 Center for Ecology and Evolutionary Ecology, Joint Research Unit of CNRS, EPHE, IRD, University Montpellier, University Paul Valéry Montpellier 3, 34293 Montpellier, France; michael.staudt@cefe.cnrs.fr
* Correspondence: sandy.bsaibes@gmail.com (S.B.); valerie.gros@lsce.ipsl.fr (V.G.)
† Current Address: Department of Chemistry, University of Oslo, 0315 Oslo, Norway.
‡ Current Address: Department of Chemistry and Environmental Research Institute, University College Cork, Cork, Ireland.

Received: 30 May 2020; Accepted: 24 June 2020; Published: 30 June 2020

Abstract: Monoterpenes (MTs) represent an important family of biogenic volatile organic compounds (BVOCs) in terms of amount and chemical diversity. This family has been extensively studied using gas chromatography (GC) and proton transfer reaction-mass spectrometry (PTR-MS). Upon recent advances with Fast Gas Chromatography (FastGC), it was also commercialized with proton transfer reaction-time of flight-mass spectrometry (PTR-ToF-MS) instruments. The combination of both techniques showed promising results in the near real-time separation of isomers, with the need of further improvements. In this study, a FastGC prototype was coupled to a conventional PTR-MS (PTR-QuadMS). Extensive laboratory experiments were performed, in order to test the system's performance and to optimize its operational parameters for MT separation. The detection limit was determined to be around 0.8–1.7 ppbv, depending on the MT. The system was afterwards deployed during a three-week field campaign in a mixed holm oak (*Quercus ilex*) forest known for its important MT emissions. MTs were measured in the incoming and the outgoing air of dynamic enclosures installed on the branches of four different trees. Three chemotypes of holm oak trees could be distinguished showing consistently different proportions of the emitted MTs throughout the measurement campaign: pinene-type, myrcene-type and limonene-type. Measurements showed a systematic diel variation in emissions typical of light and temperature-dependent, de novo-synthesized VOCs. The results demonstrated the feasibility of the FastGC/PTR-MS system for continuous measurements from dynamic chambers in the field, whereas further improvements would be necessary to lower the detection limit for ambient air measurements.

Keywords: FastGC; PTR-MS; monoterpenes; *Quercus ilex*

1. Introduction

Terrestrial vegetation, including forests, crops, grasslands and shrubs, represents the dominant source of volatile organic compounds (VOCs) released in the atmosphere. With annual global emissions estimated to be 750–1150 TgC yr^{-1}, biogenic VOCs (BVOCs) account for about 90% of total VOC emissions [1,2]. Plant-produced VOCs are of particular interest, seeing their abundance and their considerable role in gas phase and heterogeneous chemistry of the troposphere. They are subject to photochemical processes, involving atmospheric oxidants like OH, O_3 and NO that lead to the formation of a harmful tropospheric ozone and secondary organic aerosols (SOAs) [3,4]. Despite the considerable effort invested to better understand BVOC-mediated tropospheric photochemistry, substantial uncertainties still exist. These uncertainties are highlighted by discrepancies often observed between measured total OH reactivity and the estimated OH reactivity derived from simultaneous VOC measurements. The total OH reactivity is defined as the sum of the concentration of each compound, multiplied by the respective rate coefficient of the reaction with OH. These differences, noted as missing OH reactivity, are due to unmeasured or unidentified primary emitted and/or secondary formed reactive species. They highlight the need for a more detailed characterization of BVOCs, especially in forest environments where higher values of OH reactivity and missing OH reactivity were reported [5–11].

In natural ecosystems, VOCs are emitted from all plants' organs, most importantly from foliage, with a large chemical diversity. Their amount as well as their chemical composition depend inherently on the plant's genotype as well as on external biotic (plants, animals, microorganisms) and abiotic factors such as temperature, light and water availability [12]. The most prominent compound groups are isoprene and monoterpenes (MTs), estimated to represent 61–70% and 11–12%, respectively, of BVOCs' global estimated flux [2,13]. While isoprene has a single known rate coefficient with respect to atmospheric oxidants, MTs consist of multiple structural isomers with greatly varying reactivity [14]. Furthermore, they contribute to SOA formation with variable yields depending on environmental conditions, but also strongly on the BVOC structure [15]. Therefore, it is of great interest to quantify each individual MT isomer in order to achieve a better characterization of BVOCs' impact on aerosol loading and their implication in the oxidative capacity of the atmosphere. In addition, MTs were reported to be dominant in some forest ecosystems such as boreal coniferous forests or Mediterranean evergreen vegetation [16]. Given their variable emission rates and their relatively high reactivity, ambient air concentrations of MTs can show significant short-term variations, which require high time resolution measurement techniques.

Several analytical techniques have been used to characterize MT emissions from plants. Conventional gas chromatography (GC), providing detailed information regarding the chemical composition, is one of them. GC methods allow separation and quantification of MT isomers with a frequency of one measurement every 30 min to 1 h 30 min. Proton transfer reaction-mass spectrometry (PTR-MS) is a technique allowing real-time determination of MTs at low atmospheric levels (ppbv-pptv). However, PTR-MS is limited by its inability to distinguish compounds with the same molecular mass and hence MT isomers [17]. In order to combine the advantages of both techniques, GC columns were coupled to PTR-MS instruments, so different isomers could be separated [18,19]. More recently, a FastGC add-on for PTR-MS instruments was developed and deployed in the fields of food [20] and atmospheric sciences [21–23]. Indeed, PTR-MS provided real-time measurements of total MTs and the integration of the FastGC module allowed the identification and the quantification of each isomer. While Romano et al. (2014) [20] were the first to test a FastGC prototype coupled to a proton transfer reaction-time of flight-mass spectrometry (PTR-ToF-MS) instrument on wine, proving that the technique extended the analytical capabilities of the PTR-MS, Materić et al. (2015) [21] deployed the system to investigate MT emissions from plants. In their study, laboratory experiments on MT standards, Scots pine, black pine and Norway spruce samples (emissions from a small part of harvested branches or from a pair of needles) showed that this method can perform rapid separation and identification of most abundant MTs, even at low concentrations (i.e., 4–6 ppbv per individual MT from spruce). Later on, Pallozi et al.

(2016) [23] used the commercial FastGC coupled to a PTR-ToF-MS to characterize individual MT emissions from young *Quercus ilex* and *Eucalyptus camaldulensis* saplings. Their system appeared to be quite sensitive (detection limit around 68.15 μg m^{-3}, corresponding to 12.2 ppbv) but not sufficiently selective, since sabinene and β-pinene co-eluted and *D*-limonene and cis-β-ocimene were only partially separated. These studies showed that the FastGC/PTR-MS system is a promising technique for the near real-time characterization of individual MTs. They also confirmed the need for a further optimization in order to achieve a fast separation with a good resolution.

Herein, we present the adaptation of a new FastGC prototype on a conventional PTR-MS and its field deployment to measure MT emissions from *Quercus ilex* L. (holm oak). *Q. ilex* is an evergreen oak abundant in the Mediterranean area. It is known as a strong emitter of MTs, contrary to many deciduous oak species emitting large amounts of isoprene. The short-term control of MT emissions involve not only temperature but also light [24]. These conclusions were confirmed by other observations demonstrating that MTs from *Q. ilex* are formed in the chloroplast from photosynthesis intermediates, and that they are immediately emitted after synthesis without being accumulated inside leaves [25]. Using chromatographic techniques, these pilot studies showed that α-pinene, sabinene and β-pinene are the main emitted MTs, representing about 80% of total MTs [26]. However, later studies that investigated the intraspecific variability of emissions in various natural holm oak populations observed the existence of other chemotypes with a dominance of limonene or myrcene in their emission profiles [27,28].

The first section of this study presents the laboratory optimization phase of MTs measurements with the FastGC/PTR-MS, under different operational parameters. The second section describes the deployment of the system in a three-week field experiment aiming to characterize the intraspecific and diurnal variability of MT isomer emissions from *Q. ilex* foliage. Finally, the performance of the system is discussed including improvements and challenges, and the main results are compared to previous studies on MT emissions from *Q. ilex*.

2. Materials and Methods

2.1. Description of the FastGC System and Mode of Operation

In order to achieve a rapid separation of MT isomers in fast chromatographic runs (tens of seconds), a prototype version of the FastGC add-on (IONICON Analytik, Innsbruck, Austria), presented in Figure 1, was coupled to a conventional PTR-MS (IONICON Analytik, Innsbruck, Austria). This prototype is a modified version of the setup used by Ruzsanyi et al. (2013) [29] and Romano et al. (2014) [20]. It is described in Malásková et al. (2019) [30]. Briefly, a 10 m nonpolar dimethyl polysiloxane column (MXT1, RESTEK, Bellefonte, PA, USA) with an internal diameter (I.D.) of 0.53 mm and an active phase of 0.25 μm was resistively heated via a laboratory power supply (PSI 5000 A, EPS Stromversorgung GmbH, Augsburg, Germany). The latter was controlled by a microcontroller (Arduino UNO ref3, Arduino, USA). The samples were injected into a 0.5 mL sample loop made of passivated stainless steel. A two-position 10-port diaphragm valve (VICI AG, Schenkon, Switzerland) combined with a 3-way solenoid valve as the actuator, provided rapid switching between real-time measurements and chromatographic runs. The switching process was performed fully automated via the PTR-MS Control v2.7 software (IONICON Analytik, Innsbruck, Austria). Make-up gas was injected into a custom made 5-port virtual valve (FastGC inlet, Figure 1), to ensure that only the sample introduced by the carrier gas flow entered the drift tube. The major improvement in the present prototype is the replacement of the inlet valve system by a single multiport valve. This change did not only reduce the internal dead volume, but also enabled the column back-flushing during real-time measurements, since the column could be decoupled from the PTR-MS. Chemical background and memory effects were thus greatly reduced. Optimization of the materials used improved these aspects even more, resulting in a better limit of detection (LoD) and an enhanced resolution. It is worth noting that using a conventional PTR-MS gives the possibility to introduce helium (He) as the carrier

gas. Indeed, the relatively high flows inside the PTR-MS drift tube ensures that the sample matrix is predominantly composed of nitrogen (N_2), so the effect of He would remain negligible on the ion chemistry. Finally, with coupling the FastGC to the conventional PTR-MS, came some technical challenges. They included the need of very low dwell times narrowing the amount of monitored masses, the higher dilution due to the higher flow inside the PTR-MS drift-tube and the necessity to adapt a number of control elements, since the normal PTR-ToF-MS input/output system is not available. The latter was the main adaptation made in this setup, compared with the one described in Malásková et al. (2019) [30], where this FastGC prototype was coupled to a PTR-ToF-MS.

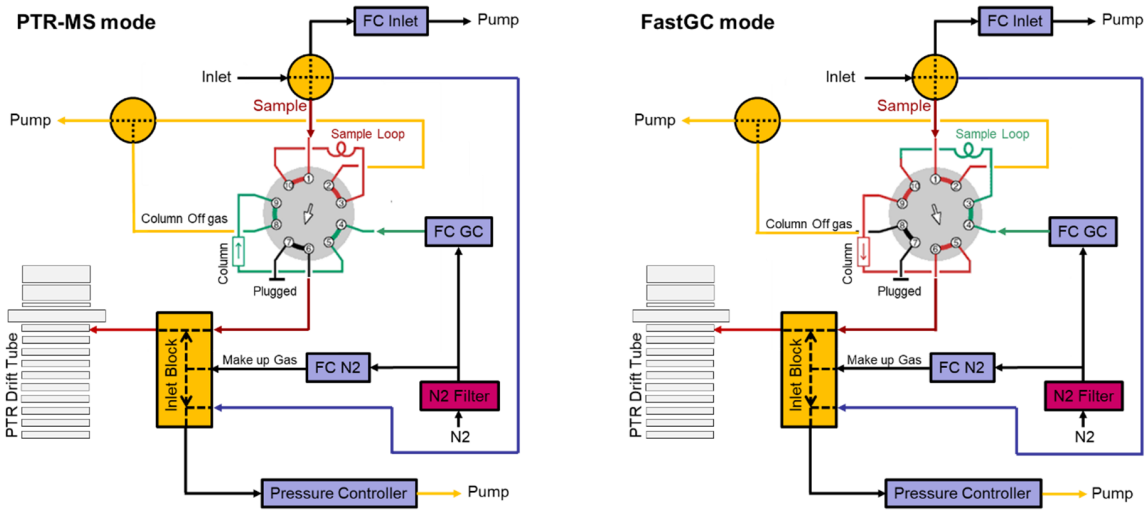

Figure 1. Schematic drawing of a proton transfer reaction-mass spectrometry (PTR-MS) instrument inlet system with a fast gas chromatography (FastGC) setup including a capillary column, a sample loop and a 10-port valve allowing the switching between real-time and FastGC measurements (Source: IONICON, Analytik, Innsbruck). FC: Flow Controller, N2: Nitrogen, GC: Gas Chromatography.

In gas chromatography, the efficiency of the separation and the quality of the resulting chromatograms can be influenced by several operational parameters, such as temperature and carrier gas flow rates. Extensive laboratory experiments were performed prior to the campaign, in order to assess the performance of the FastGC/PTR-MS system. Tests are described in the following section and their outcome are summarized in the results in Section 3.1.

2.2. Laboratory Tests and Parameters Optimization

In order to achieve a fast and satisfying separation of MTs, three main parameters were tuned: (i) the column temperature program (voltage ramp of resistance heating), (ii) the nature and (iii) the flow rate of the carrier gas. This section presents the standards used for the laboratory tests and gives an overview of the tests performed to achieve the optimal operational parameters.

2.2.1. Standards

We sampled from the headspace of individual and a mixture of five MT solutions: α-pinene (98% Sigma-Aldrich), myrcene (100%, Sigma-Aldrich), Δ_3-carene (90%, Sigma-Aldrich), limonene (99%, Sigma-Aldrich) and γ- terpinene (98.5%, Sigma-Aldrich). For individual MT samples, one to two drops of each standard were placed in a separate 2 mL glass vial, closed with a PTFE septum cap and left for a couple of minutes to equilibrate. Each vial was placed in a 1000 mL glass bottle closed with a 2-port screw cap, through which circulated zero air. A dilution system was built as shown in Supplementary Materials Figure S1. For sampling a mixture of MTs, the vials of individual MTs were placed in the same glass bottle. Another way consisted of preparing a MT gas mixture by injecting headspace samples (0.5–1 mL) of α-pinene, myrcene, Δ_3-carene, limonene and γ-terpinene in an empty clean gas canister,

previously filled with ≈1 bar of zero air and completed with ≈4 bars of N_2. A gas mixture from the National Physical Laboratory (NPL, Teddington, UK) containing 6 MTs: α-pinene (2.25 ± 0.07 ppbv), β-pinene (2.13 ± 0.11 ppbv), myrcene (2.49 ± 0.12 ppbv), Δ_3-carene (2.34 ± 0.12 ppbv), cis-β-ocimene (2.27 ppbv) and limonene (2.24 ± 0.11 ppbv), and an α-pinene gas standard (10 ppmv) were also used, mainly for quantification.

2.2.2. Overview of the Tests Performed at the Laboratory

Column temperature and carrier gas flow rates are the operational parameters that could be easily tuned for a better separation and a short analysis time, hence several combinations of these two parameters were tested (see Supplementary Materials Table S2). Briefly, a first set of experiments aimed to evaluate the effect of the temperature program on the peak shape and on each compound's retention time. Tests were initially performed with individual MT samples, and afterwards with the mixture. Each injection was repeated several times in isothermal conditions, where a constant voltage was applied (ranging between 35 and 60 V), or with the application of a temperature ramp obtained by applying a voltage gradient ("Tramp I" shown in Supplementary Materials Table S1, was initially tested). In a second set of experiments, different flow rates (ranging between 3 and 15 sccm) of N_2 as the carrier gas were tested with different temperature ramps. Helium (He) was also tested as an alternative carrier gas, which generally leads to a better separation and peak shape. Finally, a quantitative analysis was performed, using the NPL gas standard.

2.3. Field Campaign

2.3.1. Description of the Measurement Site

The ADEME-COV^{3}ER field campaign was conducted between 20 June and 11 July 2018 at the Integrated Carbon Observing System (ICOS) Puechabon experimental site (FR-Pue), located 35 km northwest of Montpellier, South of France (43°44′30″ N, 3°35′40″ E). The forest is dominated by *Q. ilex* which represents more than 80% of the vegetation. The average tree height is about 5.5 m and the density of stems is around 4700 stems ha^{-1} (2015). The main species composing the understory are *Buxus sempervirens* L., *Phyllirea latifolia* L., *Pistacia terebinthus* L. and *Juniperus oxycedrus* L. The area is characterized by a Mediterranean climate, with rainfalls during autumn and winter and dry conditions during summer [31].

2.3.2. Branch Enclosure System

In order to monitor the intra-specific diversity and diel (denoting a period of 24 h) variability of MTs emissions from *Q. ilex* foliage, two custom-made dynamic chambers were installed subsequently on small terminal branches of four different adult trees (Figure 2). The branches were located at 2 to 3 m height at the eastern and southern part of the tree crown and were composed of current-year (2018) and last-year (2017) leaf cohorts in variable proportions. The chambers had a cylindrical shape with a 15 cm diameter and a volume of approximatively 3 L. Each chamber consisted of two acrylglas rings interconnected with 3 thin metal braces that were adjusted in length to suit the branch size. Unfiltered ambient air was drawn through the chambers at flows kept between 7 and 11 L min^{-1}. A small fan with PTFE blades (motor outside) allowed the mixing of the chamber air and sustained heat exchange. Temperature and photosynthetically active radiation (PAR) were monitored continuously using a thermocouple placed inside and a quantum probe (PAR-SB 190, LI-COR, Lincoln, NE, USA) placed outside of the chamber, respectively. Further details can be found in Staudt et al. (2019) [32].

Figure 2. Photo of the branch chamber used during the Puechabon field experiment.

2.3.3. FastGC/PTR-MS Sampling System

The air going in and the air going out of the dynamic chambers were sampled through two 7 m long, $\frac{1}{4}$" OD Teflon lines. The inlet air was sampled from an independent line located close to the chambers and the outlet air was taken from the main line drowning air through the chambers. Both lines were connected to a VICI 4-port valve (V1 in Figure 3, VICI AG, Schenkon, Switzerland), allowing quick switches between the inlet and the outlet air of the chambers. While measuring in one line, the other line was continuously flushed using an extra pump (P1 in Figure 3) and vice versa. The air flow through the lines was around 1 to 1.2 L min^{-1}. Background measurements were performed using the gas calibration unit (GCU, IONICON, Analytik, Innsbruck, Austria).

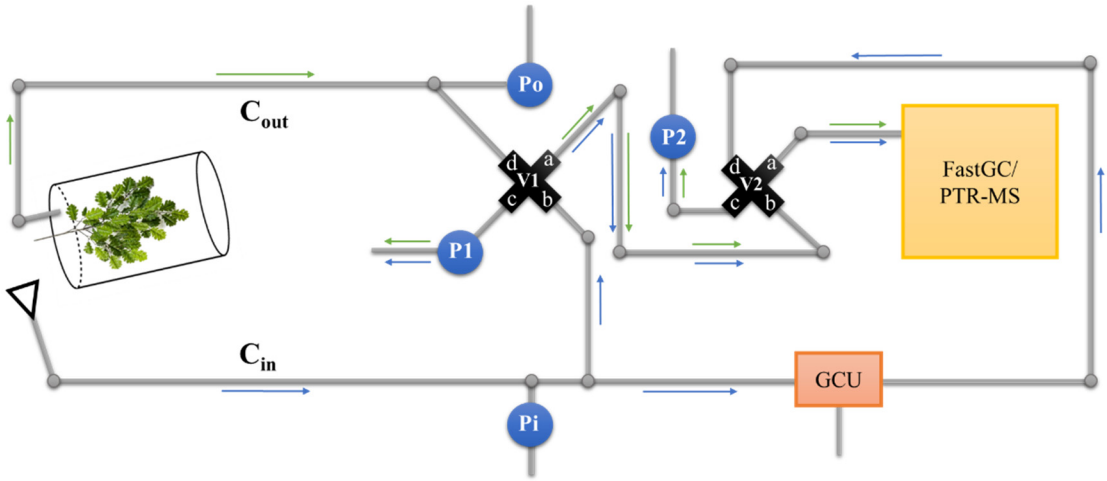

Figure 3. Schematic of the sampling system connecting a dynamic branch chamber to the FastGC/PTR-MS. Po and Pi stand for the pumps drowning the outlet and inlet air, respectively. P1 and P2 represent the flushing pumps connected to the valves V1 and V2, respectively. C_{In} and C_{Out} represent the incoming and the outgoing chamber air, respectively.

2.3.4. Measurement Program and Sequences

Continuous monitoring of MTs from holm oak branches was made during the period from 29 June to 2 July and from 6 to 8 July, 2018. Each branch emission was monitored for at least 24 h with a sequence of 10 min inlet air and 50 min outlet air measurements each hour. Each 10 min of measurements included around 7 min of real-time measurements with the PTR-MS mode and

2 min 40 s of chromatographic separation in the FastGC mode. The chromatographic run was slightly extended during the second half of the campaign, to be around 2 min 50 s.

2.3.5. FastGC/PTR-MS Operating Conditions during the Campaign

During the field experiment, the PTR-MS operational parameters were as follows: 2.2 mbar drift pressure, 600 V drift voltage and 60 °C drift tube temperature, resulting in a reduced electric field (E/N) of 131 Td (1 Td = 10^{-17} V/cm^2). The inlet line consisted of a PEEK capillary heated up to 60 °C and the inlet flow was around 100 sccm. For the FastGC, 4.2 sccm of He and 15 sccm of N_2 were used as the carrier and make-up flow, respectively. The voltage was initially ramped from 5 to 50 V within 160 s. In the second half of the campaign (for the *Q. ilex* III and IV measurements), the voltage ramp was extended to 75 V in 170 s (Table 1) in the aim to detect further potential isomers.

Table 1. Voltage ramp (estimated temperature ramp) applied for field FastGC/PTR-MS measurements. In grey, the ramp applied during the *Q. ilex* I and II measurements and the total ramp is the extended version applied for the *Q. ilex* III and IV measurements.

Time (s)	0	10	100	150	160	170	171
Voltage (V)	5	35	45	50	50	75	0
Temperature (°C)	*	63	94	111	111	223	- - -

* The ramp started at ambient temperature.

The FastGC mode was limited to *m*/*z* 21 (50 ms), *m*/*z* 32 (10 ms) and *m*/*z* 81 (200 ms) with an acquisition frequency of 3.8 Hz. MTs were monitored at *m*/*z* 81 (fragment of MTs) instead of *m*/*z* 137, given the PTR-MS higher transmission in this *m*/*z* range (Supplementary Materials Figure S3). Real-time mode measurement was on the following *m*/*z*: *m*/*z* 21 (100 ms), *m*/*z* 25 (100 ms), *m*/*z* 30 (100 ms), *m*/*z* 32 (100 ms), *m*/*z* 37 (100 ms), *m*/*z* 55 (100 ms), *m*/*z* 33 (500 ms), *m*/*z* 45 (500 ms), *m*/*z* 59 (500 ms), *m*/*z* 69 (1000 ms), *m*/*z* 71 (500 ms), *m*/*z* 73 (500 ms), *m*/*z* 81 (1000 ms), *m*/*z* 109 (500 ms) and *m*/*z* 137 (1000 ms), resulting in an acquisition frequency of 0.15 Hz.

2.3.6. System Calibration

During the campaign, the PTR-MS was calibrated for real-time measurements, and for MT chromatographic separation using the NPL standard mentioned in Section 2.2.1. The undiluted NPL gas mixture was injected daily, in order to check the retention time of each MT and their potential shifts. The sensitivity obtained for *m*/*z* 81 in the real-time measurements with the PTR-MS was 4.09 ncps/ppbv and the sensitivity ranges obtained for individual MTs in the FastGC mode (always for *m*/*z* 81) were as follows: 1.65–2.02 ncps/ppbv for α-pinene, 1.82–2.23 ncps/ppbv for β-pinene, 0.88–1.00 ncps/ppbv for myrcene, 1.38–1.72 ncps/ppbv for Δ_3-carene and 1.51–2.21 ncps/ppbv for limonene/ocimene. Since the NPL standard does not contain sabinene, a mean coefficient calculated from the obtained coefficients of α-pinene, β-pinene, myrcene, Δ_3-carene and limonene/ocimene was calculated to be 1.57–1.69 ncps/ppbv.

2.3.7. Data Analysis

Chromatograms were analyzed with custom written Matlab scripts (MATLAB R2019a, MathWorks). Since the signals recorded by the PTR-MS are rather noisy at the short dwell times used, signals were first smoothed with a 5-point Savitzky Golay filter. To account for fluctuations in the starting temperature and small delays in the automated starting of the ramp, chromatograms were aligned on the O_2^+ peak. O_2 traverses the column without interactions and is thus a good reference point. Signals were further baseline-corrected and peaks were identified with Matlab's "findpeaks" function. The threshold for peaks was set to 3-times the standard deviation plus the average obtained from the first 100 datapoints of the chromatogram. Peaks were fitted using the custom peakfit.m function assuming a Gaussian peak shape.

2.3.8. Emission Rate Calculation

In order to compare the total quantity of MTs emitted by the four branches, emission rates were calculated using Equation (1):

$$F = \frac{(C_{out}(MTs) - C_{in}(MTs)) \times Q}{DW} \quad (1)$$

where F is the *MT* emission rate expressed in μg g^{-1} (biomass dry weight) h^{-1}, C_{out}(*MTs*) and C_{in}(*MTs*) are the outlet and inlet total *MT* concentrations in μg m^{-3}, *DW* is the dry biomass (g) of the leaves inside the enclosure (determined after 2 days at 60 °C) and Q is the air flow rate in m^3 h^{-1}. The emission rates per projected leaf area ng m^{-2}(total leaf area) s^{-1} were also determined based on Equation (1), replacing *DW* (g) with leaves total area in m^2 (determined from the analysis of scanned leaves images with the Image J software) and expressing C_{out}(*MTs*) and C_{in}(*MTs*) in ng m^{-3} and Q in m^3 s^{-1}. For each one hour of measurements, C_{out} was sampled for 50 min and C_{in} for 10 min. The concentrations were therefore interpolated at common time steps prior to compute the rates.

3. Results

3.1. Optimization Phase

Extensive laboratory experiments allowed us to determine the optimal parameters for individual MT measurements with the described FastGC/PTR-MS system. The application of a voltage ramp, showed to be advantageous on the quality of the chromatographic separation, compared with isothermal conditions. Even though the latter conditions resulted in faster GC runs, it was at the expense of the peak shape quality. Indeed, some MTs such as α-pinene (Supplementary Materials Figure S2) exhibited a larger peak width and lower peak height at a constant voltage (i.e., constant temperature), reducing the resolution. Comparing tests with the same voltage program, a better separation was demonstrated using lower carrier gas flow rates in the investigated range of flows. However, lower flow rates lead to longer GC runs. This said, a compromise had to be found between a satisfying peak resolution and the duration of the GC run. Among the different tests performed with different combinations of temperature programs and carrier gas flow rates, satisfying results were obtained by applying the temperature ramp shown in Figure 4a with a carrier gas (N_2) flow rate of 3 sccm. This voltage ramp was adopted and slightly tuned for the field campaign measurements, as shown in Table 1 (Section 2.3.5) and Figure 4b. Using the optimized flow rate (3 sccm) and applying the optimized voltage ramp, a good peak shape and a faster chromatographic run were obtained with He as the carrier gas (Figure 4b), compared with the use of N_2. This was expected given that the optimal point in the van Deemter curve is at higher linear velocities for He compared with N_2, allowing higher flows for the optimum separation [33]. Therefore, He was selected as the carrier gas to use during the field campaign. It is worth noting that in a mass flow controller calibrated for N_2, a displayed flow rate of 3 sccm of He means an actual flow rate of 4.2 sccm, knowing the public standard conversion factors of 1.00 and 1.40 for N_2 and He, respectively. Regarding the limit of detection (LoD), it was as follows during the measurement campaign: 0.9 ppbv for α-pinene and limonene/ocimene, 0.8 ppbv for β-pinene, 1.0 ppbv for sabinene and 1.7 ppbv for myrcene. These values of LoD were determined as the 3σ on 10 runs of the background which correspond to the initial part of the considered chromatograms, where no peaks are expected.

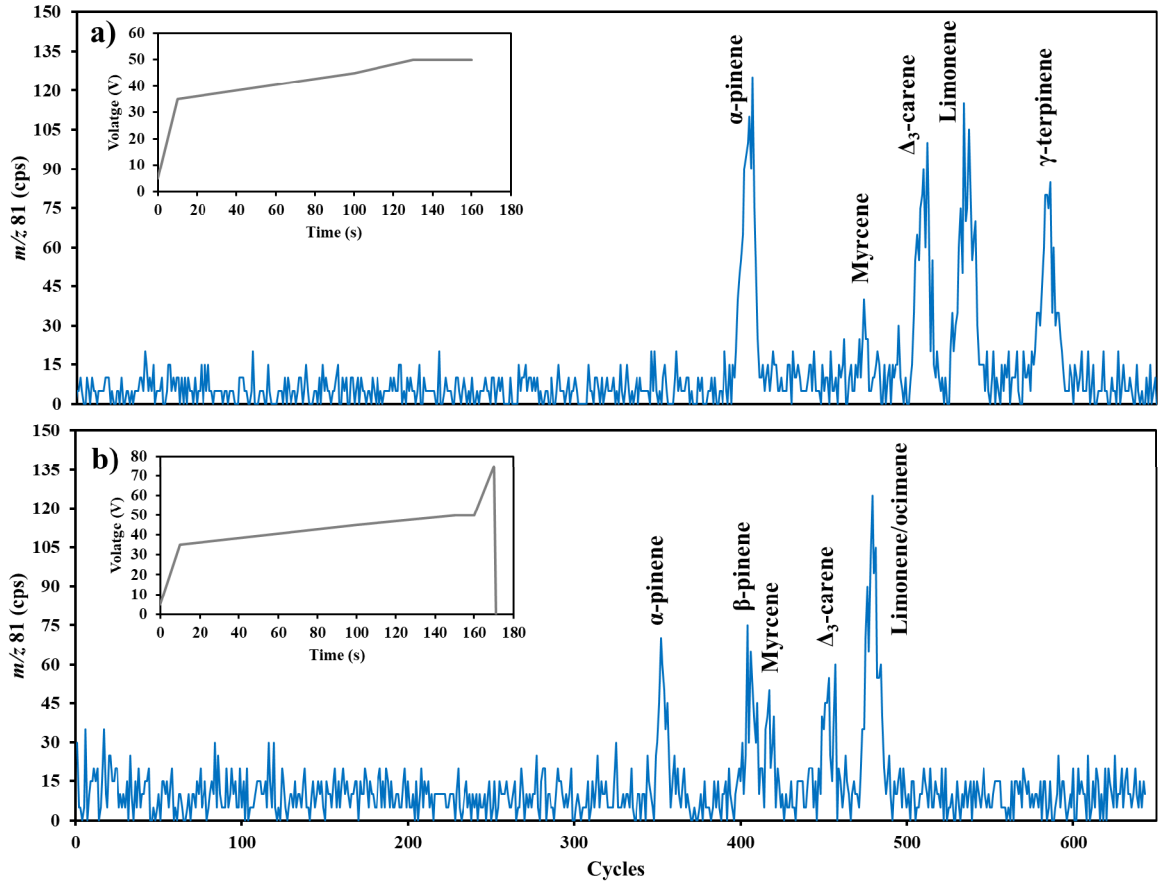

Figure 4. Chromatograms obtained when sampling (**a**) from the homemade MTs gas mixture, using 3 sccm of N_2 as the carrier gas and applying the optimal voltage ramp and (**b**) from the National Physical Laboratory (NPL) gas standard with 4.2 sccm of He as the carrier gas and applying the optimal, extended voltage ramp (Table 1).

3.2. Results from the Field Campaign

3.2.1. MTs Chemical Speciation

Figure 5 shows four FastGC chromatograms obtained from branches of the four studied trees at the same hour of different days (around 12:45 UTC). In total, six different peaks could be separated by the FastGC/PTR-MS system. Five of them were identified, from the first eluted to the last eluted peak, as α-pinene, sabinene, β-pinene, myrcene and limonene, while the last one remained unknown. However, it should be noted that the limonene peak could also have included ocimene (more specifically cis-β-ocimene), since limonene and ocimene could not be separated. Meanwhile, α-pinene, β-pinene, myrcene and limonene/ocimene were detected based on their retention times found by injecting the NPL standard mixture (Section 2.2.1), and the sabinene peak was identified based on the comparison with previous studies, where sabinene was reported to be among the major emitted MTs. When comparing the four chromatograms, we can clearly see that the main MTs were emitted in different proportions (Table 2). While the emissions of *Q. ilex* I exhibited a major peak of myrcene, those of *Q. ilex* II were dominated by α-pinene, β-pinene and sabinene in similar proportions. By contrast, the emission profiles of *Q. ilex* III and IV showed important peaks of limonene (+ocimene).

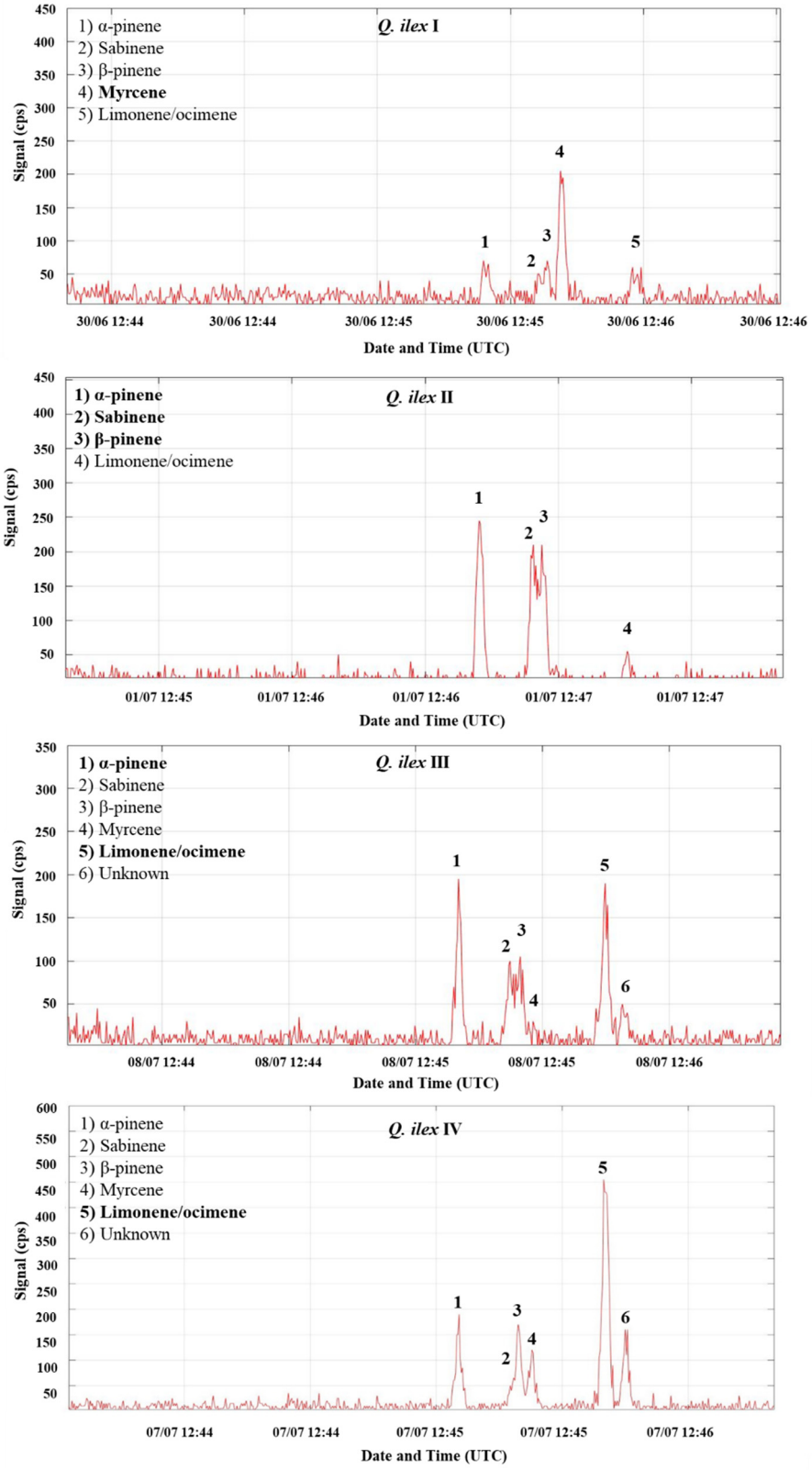

Figure 5. FastGC/PTR-MS chromatograms from the four Q. ilex branch enclosures at the same hour of different days (around 12:45 UTC). In bold are the dominant MTs for each tree.

Table 2. Summary of the operational conditions, meteorological parameters, mean and maximum emission rates of total MTs and the proportions of individual MTs for the four branch chambers.

Branch Chamber		I	II	III	IV
Measurement period		29 June–1 July	1 July–2 July	7 July–8 July	6 July–7 July
Oak chemotype		Myrcene	Pinene	Limonene	Limonene
Flow rate (L min^{-1})		10	10	8.3	8.3
Total leaf dry mass (g)		1.85	2.73	2.22	2.78
Leaf projected area (cm^2)		94	115	115	153
Temperature (°C)		15–36	16–36	16–39	15- 38
PAR (μmol m^{-2} s^{-1})		0–1691 *	0–1711 *	0–2009 #	- - - -
Emission rate (μg g^{-1} h^{-1})	Day-time maximum	50	44	68	63
	Day-time average	7	12	23	14
	24-h average	6	8	15	9
Emission rate (ng m^{-2} s^{-1})	Day-time maximum	2739	2908	3648	3178
	Day-time average	378	770	1216	697
	24-h average	330	521	812	465
MTs proportions (%)	α-pinene	16 ± 5	40 ± 4	25 ± 2	18 ± 4
	sabinene	11 ± 3	32 ± 4	21 ± 3	- - - - -
	β-pinene	10 ± 3	28 ± 4	18 ± 3	19 ± 4
	myrcene	55 ± 10	- - - - -	9 ± 3	20 ± 3
	limonene/ocimene	7 ± 3	- - - - -	27 ± 3	42 ± 8

* Recorded at oak branch I. # Recorded at oak branch III. Day-time: PAR ≠ 0 between 4:00 and 20:00 UTC. MTs proportions were calculated as the ratio of each MTs mixing ratio over the sum of all MTs detected and quantified with the FastGC/PTR-MS. These proportions correspond to the average proportion calculated for data points for when all MTs exist (measurements when one or more MTs were missing, were not considered).

The integration of the resulting chromatograms (six chromatograms/hour among which five corresponded to outgoing air samples and one to an incoming air sample) allowed us to quantify the identified individual MTs for each branch chamber. Figure 6 presents the variability of individual MT mixing ratios in the outgoing chamber air, together with the total MTs (ppbv) measured in the real-time mode and PAR data (μmol m^{-2} s^{-1}). All individual MTs followed the solar radiation profile and exhibited higher levels with higher PAR. When the branch was in the shade (i.e., branch chamber I around 11:00–12:00 UTC), all MT mixing ratios dropped down. They reached minimum levels at night. The sum of the five individual MTs (FastGC/PTR-MS) was compared to the real-time total MTs measurements (PTR-MS), showing that the detected MTs closed the budget of total MTs for *Q. ilex* I, whereas they represented around 69 ± 10%, 79 ± 8% and 76 ± 19% of total MTs for *Q. ilex* II, III and IV, respectively, indicating a missing fraction.

As mentioned before, *Q. ilex* I was characterized by a higher level of myrcene compared with pinenes. In fact, myrcene represented around 55% of the sum of MTs for this branch followed by α-pinene (16%), sabinene (11%), β-pinene (10%) and limonene (7%). For *Q. ilex* II, α-pinene was dominant almost all day long (40% of the sum of MTs) with similar levels of β-pinene and sabinene (28% and 32%, respectively). Interestingly, two different behaviors were observed for the two oak branches with high levels of limonene. For *Q. ilex* III, limonene/ocimene and α-pinene had close values (27% and 25%, respectively), with slightly higher levels of limonene/ocimene at maximum PAR (Figure 6), whereas for *Q. ilex* IV, limonene/ocimene was by far the most dominant MT (42% of the sum of MTs). A summary is presented in Table 2. These proportions generally remained similar all day long.

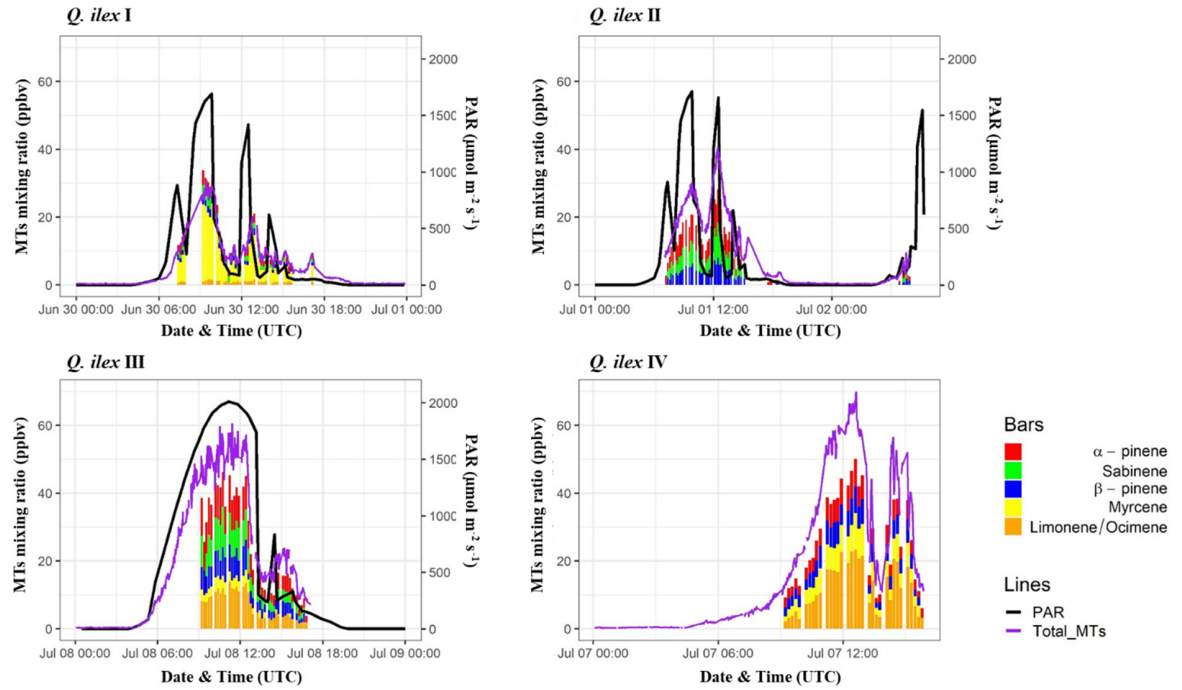

Figure 6. Diurnal variations of photosynthetically active radiation (PAR) and mixing ratios of individual MTs in the chamber air of the four studied trees. No PAR data are available for *Q. ilex* IV.

Regarding total MTs in the incoming chamber's air (ambient air), their levels were quite low (2.1 ± 1.9 ppbv on average for the whole real-time measurement period), most probably due to efficient mixing and dilution in the atmosphere. Accordingly, individual MT levels were also quite low and generally below the FastGC/PTR-MS detection limit. Thus, single MTs could hardly be detected and quantified in ambient air.

3.2.2. *Q. ilex* Total MTs Foliar Emissions

As for individual MTs, the total MTs emissions exhibited a clear diurnal cycle, showing the maxima during day-time and no emissions during night-time, following temperature and light cycles (see example for *Q. ilex* II in Figure 7 and for the other branches in Figures S4–S6). Two day-time peaks of emission rates were generally observed for each branch, similarly to the PAR variation recorded nearby the branches. At night, total MT mixing ratios were close to the limit of detection with similar values recorded in the outgoing and the incoming air (ambient air). Hence, as expected, no emissions occurred from the leaves in the dark (Figure 7). During sunrise around 04:00 UTC, MT emission levels started to increase together with incident light intensity and temperature, reached a maximum around midday and decreased subsequently in the afternoon and evening until 17:00–18:00 UTC. Even though high MTs emission rates were always recorded during day-time, their maxima occurred at slightly different moments for the different branches due to the variable position of the branches in the canopy resulting in variable shading. Table 2 summarizes the operational conditions, meteorological parameters, the maximum and average emission rates (μg g^{-1} h^{-1} and ng m^{-2} s^{-1}) recorded for each enclosure with the proportions of individual MTs. Their 24-h average emissions ranged between 6 and 15 μg g^{-1} h^{-1} (330–812 ng m^{-2} s^{-1}) with a maximum reaching 68 μg g^{-1} h^{-1} (3648 ng m^{-2} s^{-1}) for oak III. Oak III had the highest daily mean emission rate (15 μg g^{-1} h^{-1}) followed by oak IV (9 μg g^{-1} h^{-1}) and II (8 μg g^{-1} h^{-1}) and the lowest emissions were recorded for oak I (6 μg g^{-1} h^{-1}).

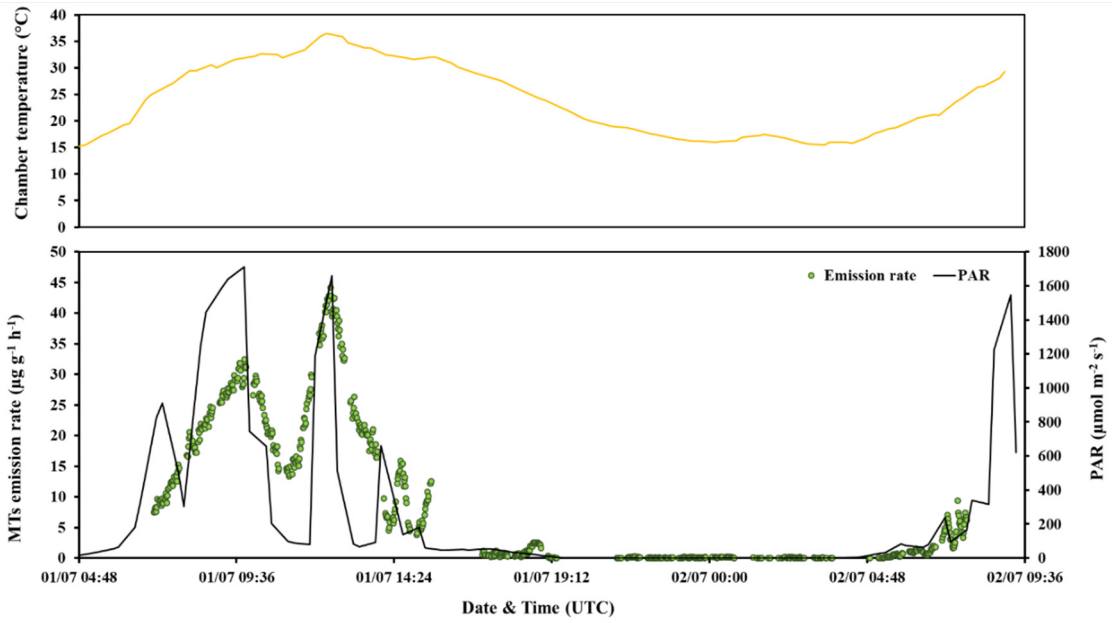

Figure 7. Diurnal variation of total MT emission rates with PAR and chamber temperature for *Q. ilex* II branch enclosure.

4. Discussion

4.1. Evaluation of the System's Efficiency to Separate MTs with a Higher Time Resolution

Calibrations and tests performed prior to the campaign, as well as those done daily during the field experiment were consistent in showing the ability of the new FastGC prototype coupled to a PTR-MS, to separate most of the main emitted MTs with fast chromatographic runs (≈160 s). In particular, the separation of sabinene and β-pinene which appeared to be quite challenging in a previous laboratory study [23], was well achieved here. However, our experiments also confirmed an insufficient resolution to separate limonene and ocimene (cis-β-ocimene) which co-eluted, producing one intense peak. This limitation in peak resolution is most probably due to the short column, its high initial temperature (30–35 °C) and the absence of a cryofocusing unit, which is useful to limit the excessive spreading of the injection band [23]. Regarding the sensitivity, it was satisfactory, given the relatively low injected sample volume (sample loop volume of 0.5 mL) compared with conventional GC instruments. The minimum detected amount of a MT peak was about 800 pptv, slightly better than the detection limit obtained in the study of Materić et al. (2015) [21], which ranged between 1.3 and 1.7 ppbv (for *m*/*z* 137) depending on the MT, using the FastGC add-on (Version 1.04) with a PTR-ToF-MS (IONICON Analytik, Innsbruck, Austria). However, some MTs in trace amounts could not be detected in the outgoing chamber air, and all MTs were hardly measured in the ambient air, which highlights this system's limitation. This limitation prevented us to monitor the diurnal concentration variations of the individual MTs in the forest air and hence to precisely calculate the individual emission rates. Several approaches could be considered to improve the detection limit of the FastGC/PTR-MS system. At the PTR-MS level, reducing measurement frequencies (applying longer dwell times) would be one of them, leading to a lower noise. However, this should be considered with care, since it can compromise the resolution and the peak shape. Another way to improve the detection limit would be by reducing the inlet flow of the PTR-MS, leading to less dilution of the carrier gas by the make-up gas. A more straightforward suggestion would consist of using a PTR-ToF-MS instrument, allowing to work at high frequencies with a lower noise compared with a conventional PTR-MS and providing an inlet flow that is ~1/3 of that of the PTR-MS, leading to a lower sample dilution. Changes can be made on the FastGC level too. The carrier gas flow rate could be increased; however, this would affect the resolution, as seen in our laboratory tests. The column could be replaced by a longer one, providing a

higher number of theoretical plates, which would lead to higher peaks for the same injected amount, as discussed in Pallozi et al. (2016) [23]. Finally, preconcentration via a cyrofocusing device can be considered which would increase both the LoD and resolution [34]. Regarding the measurements' time resolution, one FastGC data point could be obtained every 10 min during the COV3ER-2018 field campaign, including ≈2 min 40 s to 2 min 50 s of chromatographic separation and ≈7 min of real-time measurements with the PTR-MS, during which the column was cooled down to ambient temperatures.

4.2. MTs Chemical Diversity and Q. ilex Chemotypes

We detected predominantly α-pinene, sabinene, β-pinene, myrcene and limonene in the *Q. ilex* branch emissions. These compounds were already reported to be the main emitted MTs from *Q. ilex* leaves, where they can account for up to 90–100% of total MTs released [26–28,35–38]. Other MTs were reported to be emitted at low rates including α-thujene, camphene and γ-terpinene [25,28]. These compounds were not detected in our study by FastGC/PTR-MS, most probably due to their release in trace amounts. However, one of them could be the unknown/ unidentified extra compound detected in the *Q. ilex* III and IV foliar emissions. Based on boiling points, the most likely candidate is γ-terpinene.

Comparison of the MT emission signatures between the four enclosed oak branches showed differences with respect to the proportions of the five major compounds, allowing to distinguish between three main chemotypes known for holm oak and other MT emitting oak species [27,28,39]. In addition to the myrcene-type, the limonene-type and the pinene-type, an intermediate pinene/limonene-type has been observed in diverse oak populations (e.g., [27]), whose profile resembles to that of *Q. ilex* III. Biochemical studies have shown that different isomers of MT synthases exist in *Q. ilex* foliage, each one producing a specific blend of MTs [40,41]. Furthermore, diverse field and laboratory investigations demonstrated that the terpene composition produced in vitro or in vivo by the leaves of a given *Q. ilex* tree changes little with temperature or light treatments [35,42], drought and seasons [43–45] and leaf age or leaf position [28], emphasizing that the different chemical profiles released by trees are largely under genetic control. Individual MTs proportions for each chemotype were close to the ranges reported by previous studies [26,27,45].

Finally, and as demonstrated in the graphs of Figure 6, the sum of individual MTs detected by the FastGC was in the same order of magnitude of total MTs measured by the PTR-MS, with a closed budget for *Q. ilex* I and a missing fraction (25% on average) for *Q. ilex* II, III and IV. It should be kept in mind that the sensitivity obtained for myrcene was much lower than those of the other MTs. This could be explained by the linear structure of myrcene, compared with the other MTs having a C6 ring. The latter produces an *m*/*z* 81 ion after fragmentation, whereas Kari et al. (2018) [46] reported a lower fragmentation at *m*/*z* 81 for myrcene compared with α- and β-pinene, in the PTR-ToF-MS, which would probably be also the case in our PTR-MS. Alternatively, the pinene and limonene chemotypes produce a larger number of minor overseen MTs than the myrcene chemotype, or other BVOCs such as sesquiterpenes or oxygenated BVOCs (hexenal, eucalyptol) that are reported to fragment at *m*/*z* 81 [46,47]. For *Q. ilex* III and IV, we tried to consider the unknown detected isomer in the calculation of the sum of MTs by FastGC/PTR-MS, using sabinene's estimated sensitivity coefficient. This extra compound could explain 7% and 11% of the missing fraction of total MTs, for *Q. ilex* III and IV, respectively, showing that the FastGC/PTR-MS measurements are covering the main emitted compounds by *Q. ilex* (which represent 90–100% of MTs emissions).

4.3. MTs Emission Rates

MT emissions exhibited a clear diurnal cycle following light and temperature profiles. This observation is a clear evidence that MT emissions from holm oak leaves are light- and temperature-dependent, which is in agreement with many previous studies on *Q. ilex* [26,38]. This light-dependency is due to the de novo synthesis of MTs from photosynthetic products inside the chloroplasts, and due to the absence of specialized structures for terpene storage, contrary to most MT-emitting plants [25]. On a leaf-dry mass

basis as well as on a leaf-area basis, the mean emission and maximum emission rates observed in our study are in the range of those reported in previous studies on *Q. ilex* [28,44]. Finally, differences were noted in MTs emission rates, between the four studied branches. These differences could be linked to genotypic and phenological factors, specific for each branch and/or tree as well as to external factors, in this case temperature and solar radiation received by the branches.

5. Conclusions

Using a conventional PTR-MS, an adapted prototype of a FastGC was added and optimized for the separation of MT isomers and tested under real field conditions to monitor, with a fine time resolution, MTs emissions from holm oak foliage. The results highlight the ability of the FastGC/PTR-MS system to provide an online separation and detection of individual MTs. Using helium as the carrier gas and an optimized voltage ramp (temperature program), we were able to monitor the temporal variation of five MTs: α-pinene, sabinene, β-pinene, myrcene and limonene (+ocimene) with a data point every 10 min. However, even though our system was able to separate sabinene and β-pinene, which was an issue in a previous study [23], the resolution could be further improved, since limonene still co-eluted with at least one ocimene isomer. In addition, the FastGC/PTR-MS used in this study had a relatively high detection limit, and therefore hardly detected low levels of individual MTs in ambient air. Despite these limitations, near real-time chromatographic separation allowed to monitor fast changes in individual MT emissions from enclosure systems and revealed the presence of three different chemotypes: (i) pinene-type for which MT emissions are dominated by α-pinene, β-pinene and sabinene; (ii) myrcene-type, for which myrcene is the major emitted MT and (iii) limonene-type, exhibiting higher levels of limonene. These results agree with previous observations showing that the compositional fingerprint of MT emissions from *Q. ilex* is largely genetically fixed, while the released quantities undergo strong diurnal variations driven by temperature and the solar radiation received by the leaves.

In its present state, the FastGC/PTR-MS system demonstrated a good performance regarding MTs measurements from dynamic enclosures. Therefore, it could be deployed in parallel with OH reactivity measurements conducted on a chamber scale, providing high time resolution data on individual MTs. This can lower the uncertainties related to the MTs reactivity calculation, allowing a more precise estimation of the missing OH reactivity. However, the performance of the system should be further optimized in order to gain in sensitivity and resolution, so it could also be deployed in the measurement of individual ambient MTs profiles, for example. Improvement can be made by changing the column (length, internal diameter, the type and thickness of the stationary phase) and developing new FastGC (carrier gas flow rates, temperature ramps, etc.) and PTR-MS methods (longer dwell times, less sample dilution, etc.).

Supplementary Materials: The following are available online at http://www.mdpi.com/2073-4433/11/7/690/s1, Figure S1. Schematic of the sampling system built for laboratory FastGC/PTR-MS experiments on MT standards, Table S1. Summary of the tested voltage ramps (temperature programs), Table S2. Summary of the different combinations of voltage ramps and carrier gas flow rates tested during laboratory tests, Figure S2. FastGC/PTR-MS chromatograms after the injection of an α-pinene sample. *m/z* 32 and m/z 137 refer to O2 and α-pinene, respectively, Figure S3. Mass transmission from the injection of the GCU gas standard with the fitting curve by an exponential function. Figure S4. Total MTs emission rate for *Q. ilex* I branch chamber, Figure S5. Total MTs emission rate for *Q. ilex* III branch chamber, Figure S6. Total MTs emission rate for *Q. ilex* IV branch chamber.

Author Contributions: Methodology, S.B. and F.P.; software, F.P.; validation, S.B. and F.T.; formal analysis, S.B., F.P. and F.T.; investigation, S.B. and M.S.; resources, F.P., V.G., F.T., F.L., R.C., J.K., B.L. and M.S.; data curation, S.B., F.T., F.L., M.S.; writing—original draft preparation, S.B.; writing—review and editing, S.B., F.P., V.G., F.L., R.C., P.B., J.K., B.L. and M.S.; visualization, S.B. and P.B.; supervision, V.G.; project administration, B.L.; funding acquisition, B.L. All authors have read and agreed to the published version of the manuscript.

Funding: This research was funded by ADEME (COV3ER, n°1562C0032) project.

Acknowledgments: The authors acknowledge the European Union's Horizon 2020 research and innovation program under the Marie-Sklodowska-Curie grant agreement No 674911- IMPACT, the EU ICOS Research Infrastructure, ANAEE-FR services (ANR project n°11-INBS-0001), the CNRS and the CEA. We would also like

to thank Jean-Eudes Petit (LSCE), Nicolas Bonnaire (LSCE), Karim Piquemal, David Degueldre and Jean-Marc Ourcival (all CEFE) for their technical assistance.

Conflicts of Interest: The authors declare no conflict of interest. The funders had no role in the design of the study; in the collection, analyses, or interpretation of data; in the writing of the manuscript, or in the decision to publish the results.

References

1. Guenther, A.; Hewitt, C.; Erickson, D.; Fall, R.; Geron, C.; Graedel, T.; Harley, P.; Klinger, L.; Lerdau, M.; Mckay, W.; et al. A global model of natural volatile organic compound emissions. *J. Geophys. Res. Atmos.* **1995**, *100*, 8873–8892. [CrossRef]
2. Sindelarova, K.; Granier, C.; Bouarar, I.; Guenther, A.; Tilmes, S.; Stavrakou, T.; Müller, J.; Kuhn, U. Global data set of biogenic VOC emissions calculated by the MEGAN model over the last 30 years. *Atmos. Chem. Phys.* **2014**, *14*, 9317–9341. [CrossRef]
3. Curtis, L.; Rea, W.; Smith-Willis, P.; Fenyves, E.; Pan, Y. Adverse health effects of outdoor air pollutants. *Environ. Int.* **2006**, *32*, 815–830. [CrossRef] [PubMed]
4. Hallquist, M.; Wenger, J.C.; Baltensperger, U.; Rudich, Y.; Simpson, D.; Claeys, M.; Dommen, J. The formation, properties and impact of secondary organic aerosol: Current and emerging issues. *Atmos. Chem. Phys.* **2009**, *9*, 5155–5236. [CrossRef]
5. Sinha, V.; Williams, J.; Lelieveld, J.; Ruuskanen, T.M.; Kajos, M.K.; Patokoski, J.; Hellen, H.; Hakola, H.; Mogensen, D.; Boy, M.; et al. OH reactivity measurements within a boreal forest: Evidence for unknown reactive emissions. *Environ. Sci. Technol.* **2010**, *44*, 6614–6620. [CrossRef]
6. Nölscher, A.C.; Williams, J.; Sinha, V.; Custer, T.; Song, W.; Johnson, A.M.; Axinte, R.; Bozem, H.; Fischer, H.; Pouvesle, N.; et al. Summertime total OH reactivity measurements from boreal forest during HUMPPA-COPEC 2010. *Atmos. Chem. Phys.* **2012**, *12*, 8257–8270. [CrossRef]
7. Mao, J.; Ren, X.; Zhang, L.; Van Duin, D.M.; Cohen, R.C.; Park, J.H.; Goldstein, A.H.; Paulot, F.; Beaver, M.R.; Crounse, J.D.; et al. Insights into hydroxyl measurements and atmospheric oxidation in a California forest. *Atmos. Chem. Phys.* **2012**, *12*, 8009–8020. [CrossRef]
8. Hansen, R.F.; Griffith, S.M.; Dusanter, S.; Rickly, P.S.; Stevens, P.S.; Bertman, S.B.; Carroll, M.A.; Erickson, M.H.; Flynn, J.H.; Grossberg, N.; et al. Measurements of total hydroxyl radical reactivity during CABINEX 2009—Part 1: Field measurements. *Atmos. Chem. Phys.* **2014**, *14*, 2923–2937. [CrossRef]
9. Nölscher, A.C.; Yañez-Serrano, A.M.; Wolff, S.; De Araujo, A.C.; Lavrič, J.V.; Kesselmeier, J.; Williams, J. Unexpected seasonality in quantity and composition of Amazon rainforest air reactivity. *Nat. Commun.* **2016**, *7*, 1–12. [CrossRef] [PubMed]
10. Zannoni, N.; Gros, V.; Sarda Esteve, R.; Kalogridis, C.; Michoud, V.; Dusanter, S.; Sauvage, S.; Locoge, N.; Colomb, A.; Bonsang, B. Summertime OH reactivity from a receptor coastal site in the Mediterranean Basin. *Atmos. Chem. Phys.* **2017**, *17*, 12645–12658. [CrossRef]
11. Bsaibes, S.; Al Ajami, M.; Mermet, K.; Truong, F.; Batut, S.; Hecquet, C.; Dusanter, S.; Léornadis, T.; Sauvage, S.; Kammer, J.; et al. Variability of hydroxyl radical (OH) reactivity in the Landes maritime pine forest: Results from the LANDEX campaign 2017. *Atmos. Chem. Phys.* **2020**, *20*, 1277–1300. [CrossRef]
12. Penuelas, J.; Llusia, J. The complexity of factors driving voltaile organic compound emissions by plants. *Biol. Plant.* **2001**, *4*, 481–487. [CrossRef]
13. Messina, P.; Lathière, J.; Sindelarova, K.; Vuichard, N.; Granier, C.; Ghattas, J.; Cozic, A.; Hauglustaine, D.A. Global biogenic volatile organic compound emissions in the ORCHIDEE and MEGAN models and sensitivity to key parameters. *Atmos. Chem. Phys.* **2016**, *16*, 14169–14202. [CrossRef]
14. Atkinson, R.; Arey, J. Gas-phase tropospheric chemistry of biogenic volatile organic compounds: A review. *Atmos. Environ.* **2003**, *37*, 197–219. [CrossRef]
15. Lee, A.; Goldstein, A.H.; Kroll, J.H.; Ng, N.L.; Varutbangkul, V.; Flagan, R.C.; Seinfeld, J.H. Gas-phase products and secondary aerosol yields from the photooxidation of 16 different terpenes. *J. Geophys. Res. Atmos.* **2006**, *111*, 1–25. [CrossRef]
16. Kesselmeier, J.; Staudt, M. Biogenic volatile organic compounds (VOC): An overview on emission, physiology and ecology. *J. Atmos. Chem.* **1999**, *33*, 23–88. [CrossRef]

17. De Gouw, J.; Warneke, C. Measurements of Volatile Organic Compounds in the earth's atmosphere using Proton- Transfer- reaction Mass Spectrometry. *Mass Spectrom. Rev.* **2007**, *26*, 223–257. [CrossRef]
18. De Gouw, J.; Warneke, C.; Karl, T. Sensitivity and specificity of atmospheric trace gas detection by proton-transfer-reaction mass spectrometry. *Int. J. Mass Spectrom.* **2003**, *224*, 365–382. [CrossRef]
19. Warneke, C.; De Gouw, J.; Kuster, W.D.; Goldan, P.; Ray, F. Validation of Atmospheric VOC Measurements by Proton-Transfer- Reaction Mass Spectrometry Using a Gas-Chromatographic Preseparation Method Validation of Atmospheric VOC Measurements by Proton-Transfer- Reaction Mass Spectrometry Using a Gas-Chromatographi. *Environ. Sci. Technol.* **2003**, *37*, 2494–2501. [CrossRef]
20. Romano, A.; Fischer, L.; Herbig, J.; Campbell-Sills, H.; Coulon, J.; Lucas, P.; Cappellin, L.; Biasioli, F. Wine analysis by FastGC proton-transfer reaction-time-of-flight-mass spectrometry. *Int. J. Mass Spectrom.* **2014**, *369*, 81–86. [CrossRef]
21. Materić, D.; Lanza, M.; Sulzer, P.; Herbig, J.; Bruhn, D.; Turner, C.; Mason, N.; Gauci, V. Monoterpene separation by coupling proton transfer reaction time-of-flight mass spectrometry with fastGC. *Anal. Bioanal. Chem.* **2015**, *407*, 7757–7763. [CrossRef] [PubMed]
22. Papurello, D.; Silvestri, S.; Tomasi, L.; Belcari, I.; Biasioli, F.; Santarelli, M. Natural Gas Trace Compounds Analysis with Innovative Systems: PTR-ToF-MS and FASTGC. *Energy Procedia* **2016**, *101*, 536–541. [CrossRef]
23. Pallozzi, E.; Guidolotti, G.; Ciccioli, P.; Brilli, F.; Feil, S.; Calfapietra, C. Does the novel fast-GC coupled with PTR-TOF-MS allow a significant advancement in detecting VOC emissions from plants? *Agric. For. Meteorol.* **2016**, *216*, 232–240. [CrossRef]
24. Staudt, M.; Seufert, G. Light-Dependent Emission of Monoterpenes by Holm Oak (*Quercus ilex* L.) Light-dependent Emission of Monoterpenes by Holm Oak (*Quercus ilex* L.). *Naturwissenschaften* **1995**, *82*, 89–92. [CrossRef]
25. Loreto, F.; Ciccioli, P.; Brancajleoni, E.; Cecinato, A.; Frattoni, M.; Sharkey, T.D. Different sources of reduced carbon contribute to form three classes of terpenoid emitted by *Quercus ilex* L. leaves. *Proc. Natl. Acad. Sci. USA* **1996**, *93*, 9966–9969. [CrossRef]
26. Bertin, N.; Staudt, M.; Hansen, U.; Seufert, G.; Ciccioli, P.; Foster, P.; Fugit, J.L.; Torres, L. Diurnal and seasonal course of monoterpene emissions from *Quercus ilex* (L.) under natural conditions-Application of light and temperature algorithms. *Atmos. Environ.* **1997**, *31*, 135–144. [CrossRef]
27. Staudt, M.; Mir, C.; Joffre, R.; Rambal, S.; Bonin, A.; Landais, D.; Lumaret, R. Stands and Mixed Contrasting Interspecific Genetic Introgression. *New Phytol.* **2004**, *163*, 573–584. [CrossRef]
28. Staudt, M.; Joffre, R.; Rambal, S.; Staudt, M.; Mandl, N.; Joffre, R.; Rambal, S. Intraspecific variability of monoterpene composition emitted by *Quercus ilex* leaves Scaling-up WUE from leaf to canopy View project VOC emission diversity in oaks View project Intraspecific variability of monoterpene composition emitted by Quercus ilex le. *Can. J. For. Res.* **2001**, *31*, 174–180.
29. Ruzsanyi, V.; Fischer, L.; Herbig, J.; Ager, C.; Amann, A. Multi-capillary-column proton-transfer-reaction time-of-flight mass spectrometry. *J. Chromatogr. A* **2013**, *1316*, 112–118. [CrossRef]
30. Malásková, M.; Olivenza-León, D.; Piel, F.; Mochalski, P.; Sulzer, P.; Jürschik, S.; Mayhew, C.A.; Märk, T.D. Compendium of the reactions of H3O+ with selected ketones of relevance to breath analysis using proton transfer reaction mass spectrometry. *Front. Chem.* **2019**, *7*, 1–14. [CrossRef]
31. CEFE, C. Site Expérimental de Puéchabon. Available online: https://puechabon.cefe.cnrs.fr/ (accessed on 29 June 2020).
32. Staudt, M.; Byron, J.; Piquemal, K.; Williams, J. Compartment specific chiral pinene emissions identified in a Maritime pine forest. *Sci. Total Environ.* **2019**, *654*, 1158–1166. [CrossRef] [PubMed]
33. Ham, B.M.; MaHam, A. *Analytical Chemistry: A Chemist and Laboratory Technician's Toolkit*; John Wiley: Hoboken, NJ, USA, 2015.
34. Wilson, R.B.; Fitz, B.D.; Mannion, B.C.; Lai, T.; Olund, R.K.; Hoggard, J.C.; Synovec, R.E. High-speed cryo-focusing injection for gas chromatography: Reduction of injection band broadening with concentration enrichment. *Talanta* **2012**, *97*, 9–15. [CrossRef] [PubMed]
35. Staudt, M.; Bertin, N. Light and temperature dependence of the emission of cyclic and acyclic monoterpenes from holm oak (*Quercus ilex* L.) leaves. *Plant Cell Environ.* **1998**, *21*, 385–395. [CrossRef]
36. Sabillón, D.; Cremades, L.V. Diurnal and seasonal variation of monoterpene emission rates for two typical Mediterranean species (*Pinus pinea* and *Quercus ilex*) from field measurements-Relationship with temperature and PAR. *Atmos. Environ.* **2001**, *35*, 4419–4431. [CrossRef]

37. Peñuelas, J.; Llusià, J. Short-term responses of terpene emission rates to experimental changes of PFD in Pinus halepensis and *Quercus ilex* in summer field conditions. *Environ. Exp. Bot.* **1999**, *42*, 61–68. [CrossRef]
38. Ciccioli, P.; Fabozzi, C.; Brancaleoni, E.; Cecinato, A.; Frattoni, M.; Loreto, F.; Kesselmeier, J.; Schäfer, L.; Bode, K.; Torres, L.; et al. Use of the isoprene algorithm for predicting the monoterpene emission from the Mediterranean holm oak *Quercus ilex* L.: Performance and limits of this approach. *J. Geophys. Res. Atmos.* **1997**, *102*, 23319–23328. [CrossRef]
39. Welter, S.; Bracho-Nuñez, A.; Mir, C.; Zimmer, I.; Kesselmeier, J.; Lumaret, R.; Schnitzler, J.P.; Staudt, M. The diversification of terpene emissions in Mediterranean oaks: Lessons from a study of *Quercus suber*, *Quercus canariensis* and its hybrid *Quercus afares*. *Tree Physiol.* **2012**, *32*, 1082–1091. [CrossRef]
40. Fischbach, R.J.; Zimmer, I.; Steinbrecher, R.; Pfichner, A.; Schnitzler, J.P. Monoterpene synthase activities in leaves of *Picea abies* (L.) Karst. and *Quercus ilex* L. *Phytochemistry* **2000**, *54*, 257–265. [CrossRef]
41. Fischbach, R.J.; Zimmer, W. Isolation and functional analysis of a cDNA encoding a myrcene synthase from holm oak (*Quercus ilex* L.). *Eur. J. Biochem.* **2001**, *5638*, 5633–5638. [CrossRef]
42. Staudt, M.; Joffre, R.; Rambal, S. How growth conditions affect the capacity of *Quercus ilex* leaves to emit monoterpenes. *New Phytol.* **2003**, *158*, 61–73. [CrossRef]
43. Fischbach, R.J.; Staudt, M.; Zimmer, I.; Rambal, S.; Schnitzler, J.P. Seasonal pattern of monoterpene synthase activities in leaves of the evergreen tree *Quercus ilex*. *Physiol. Plant.* **2002**, *114*, 354–360. [CrossRef] [PubMed]
44. Staudt, M.; Rambal, S.; Joffre, R.; Kesselmeier, J. Impact of drought on seasonal monoterpene emissions from *Quercus ilex* in southern France. *J. Geophys. Res. Atmos.* **2002**, *107*. [CrossRef]
45. Lavoir, A.V.; Staudt, M.; Schnitzler, J.P.; Landais, D.; Massol, F.; Rocheteau, A.; Rodriguez, R.; Zimmer, I.; Rambal, S. Drought reduced monoterpene emissions from the evergreen Mediterranean oak *Quercus ilex*: Results from a throughfall displacement experiment. *Biogeosciences* **2009**, *6*, 1167–1180. [CrossRef]
46. Kari Fragmentation of myrcene, a-humulene, trans-caryophyllene at m69. *Int. J. Mass Spectrom.* **2018**, *430*, 87–97.
47. Pang, X. Biogenic volatile organic compound analyses by PTR-TOF-MS: Calibration, humidity effect and reduced electric field dependency. *J. Environ. Sci.* **2015**, *32*, 196–206. [CrossRef] [PubMed]